

Numerical Modeling of GFRP Structures under Fire Loading

B. Aguirre^{1,2}, L. Stainier¹, C. Tiago², J. Correia²

¹ GeM, École Centrale Nantes, Nantes Université, {bruno.aguirre-tessaro, laurent.stainier}@ec-nantes.fr

² CERIS, Instituto Superior Técnico, Univ. Lisboa, {bruno.tessaro, carlos.tiago, joao.ramoa.correia}@tecnico.ulisboa.pt

Abstract — A model is proposed for the simulation of the thermo-mechanical behaviour pultruded Glass Fibre Reinforced Polymer (GFRP) profiles subjected to the action of a standard fire curve. It consists of two sequential steps: (i) determination of the temperature distribution over time in a representative cross section using a thermal model that includes conduction, convection, radiation and (ii) determination of generalised strains and displacements through a mechanical model that represents the section walls through a geometrically exact shell theory using large deformations 3D constitutive relations. The problem is solved numerically using the Finite Element Method (FEM). The independently approximated fields are: temperature, pressure, velocity, decomposition, displacements, rotations and thickness variation parameters.

Keywords — thermo-mechanics, coupled problems, shells, pultruded GFRP profiles, fire resistance.

1 Introduction

Composite materials have imposed themselves in several industries over the last decades due to a set of unique characteristics, such as their self-weight, strength, insulation, low maintenance and durability. Their usage is already well widespread in several industries, *e.g.*, aerospace, automotive and marine. However, its application in civil engineering structures is still very limited when compared with the traditional solutions relying on reinforced concrete and steel elements. Among the factors that limit their use is the difficulty in guaranteeing its resistance for a certain minimum time in a fire scenario.

This article presents a model for the analysis of pultruded GFRP profiles subjected to thermal and mechanical actions. Schematic examples of such profiles are shown in Figure 1. More precisely, it intends to study simply supported beams subjected to a standard fire curve at the bottom face (in between the supports) and subjected to the action of two concentrated loads applied over the top face.

This type of beam can assume different roles in structural applications, such as the rehabilitation of pavement slabs. In rehabilitation operations of old buildings, the need to replace the original wooden floors is frequent due to their time degradation. The replacement by reinforced concrete slabs or other traditional solutions presents several disadvantages in relation to the use of GFRP profiles, such as:

- (i) an increase in the loads transmitted by the slab to the original masonry walls that would inevitably lead to the need of strengthen other structural members, such as load-bearing walls;
- (ii) more complex execution and more demanding in terms of manpower associated with the need for concreting operations or handling steel beams.

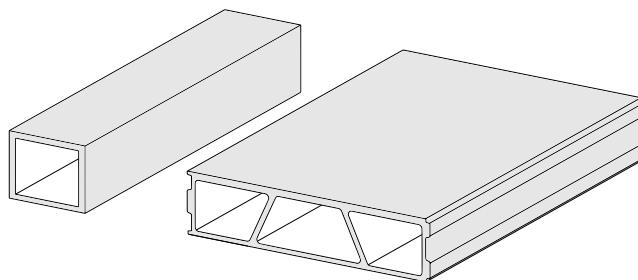


Figure 1: Example of GFRP beam profiles.

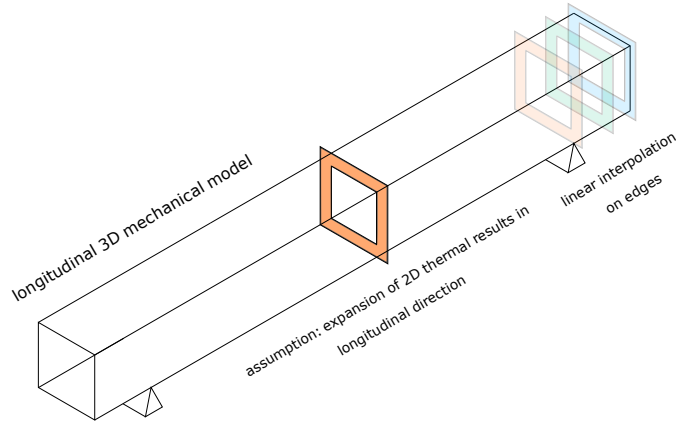


Figure 2: Schematic representation of the thermo-mechanical model.

The model presented here is the result of several years of research [1] and has been subsequently refined over this period. After a certain point it became clear that, in the case of cellular sections, the air convection in the cells and especially the internal radiation between the cell walls played a non-negligible role in the temperature distribution of tubular GFRP profiles. Thus, the most coherent approach would be to simulate the beam plus the air assembly in the cells in a three-dimensional integrated FEM model. However, this model presents some disadvantages:

- (i) the high cost in terms of computational time, since the air in the cells and the beam itself would be discretized with 3D finite elements;
- (ii) the complexity of making parametric analysis of the model, varying the beam cross section, span, loading, fire curve, protection system (size, material, thickness), *etc.*

It was also found through three-dimensional Computational Fluid Dynamics (CFD) simulations that the air movement in the longitudinal beam direction is not significant and its influence on the temperature distribution in the cross section is negligible [2]. Thus, two simplifications have been introduced:

- (i) the temperature does not vary in the longitudinal direction between the supports. Thus, a coupled 2D thermal-fluid model representing a typical cross-section is sufficient to provide the temperatures along the duration of the fire at every point of the beam. A schematic example is presented in Figure 2 for a square tubular beam;
- (ii) since the thickness of the beam walls is much smaller than the other dimensions, the three-dimensional continuum is replaced by a geometrically exact shell model.

Both problems are tackled using the FEM for the spatial discretization, whereas the finite difference method (FDM) is used along the time dimension.

A constitutive relation is proposed for the description of GFRP composites behaviour under elevated temperatures considering its anisotropic nature. The adopted simulation setup was inspired on previously performed experiments [3].

2 Thermal model

Figure 3 represents a typical cross-section of a beam, in this case a single-cell square cross-section. It illustrates the problem and the phenomena involved.

The beam is subjected to a temperature at its bottom face, the lateral faces are insulated with rock-wool, and the temperature at the upper face is the ambient one.

The set of phenomena involved is large enough for us to refrain from exposing all the equations involved. In the solid part it is admitted that the heat is transmitted by conduction. On the lower and upper faces we have boundary conditions of convection and external radiation. On the side faces it is assumed that the heat flux is null, *i.e.*, they are adiabatic boundaries. On all interior walls it is assumed

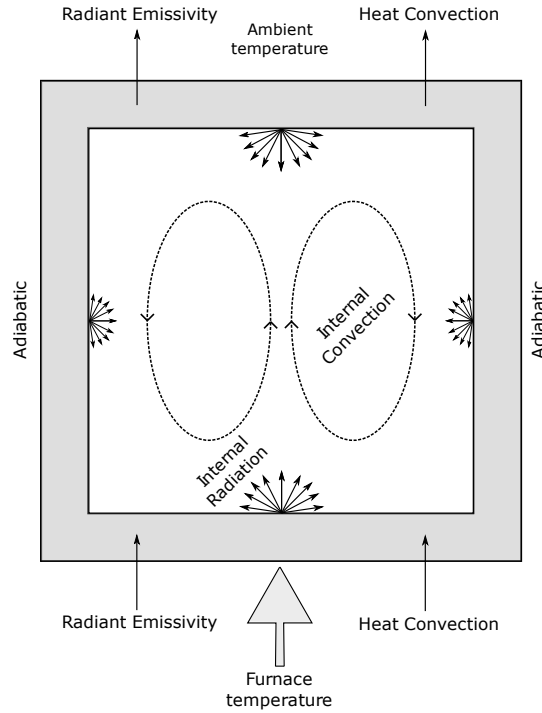


Figure 3: 2D thermal model, including conduction in the solid, convection in the fluid and internal radiation in the enclosure walls.

that the temperature in the solid and in the air are equal and that the velocity of the fluid in the cavity is null. It is also assumed that there is internal radiation in-between all walls. The fluid is assumed to be incompressible and the Boussinesq approximation is introduced, providing the artificial linear variation of the density with the temperature.

The variables of the problem are: the temperature in the fluid and solid, the pressure and velocity in the fluid and the radiosity along the inner surface of the enclosure walls. The fluid is discretized into 2D Taylor-Hood elements, the solid is discretized into quadratic 2D Lagrange elements and the radiosity are quadratic 1D elements.

An implicit first-order time integration scheme is employed. The resulting problem is solved, at each time step, using the Newton-Raphson iterative method. There are two sources of nonsymmetry in the respective tangent operator: convection and internal radiation. Moreover, the latter gives rise to dense matrices, as each one of the radiosity elements radiate to all the remaining ones.

3 Structural model

3.1 Thick shells

Historically, the approach to the problem of structural analysis of plates and shells has been based on the observation that one of the dimensions is much smaller than the remaining ones. In addition to provide a starting basis for the kinematic hypothesis on which the generalized displacement field is based, it is also the reason why the constitutive relationship of the material is subject to a static constraint, through which the so-called *plane state of stress* is imposed. Basically, an equation that reduces the number of generalized stresses/strains is introduced in the constitutive relation of the three-dimensional continuum. In order to take advantage of a true 3D constitutive law and use the full capabilities of Matlab [4], in the present work it was chosen not to introduce any hypothesis about the distribution of stresses. The price to pay for this option is the introduction into the kinematic hypothesis of the shell of the thickness variation possibility. Note that this hypothesis avoids the usual contradiction between what is assumed for the kinematics and statics of the shell.

In the following a very brief outline of the theory is provided.

Consider the schematic representation exhibited in Figure 4. The reference, initial and current configurations are denoted Ω_r , Ω_o and Ω , respectively. The vectors e_i^r represent the reference configurations

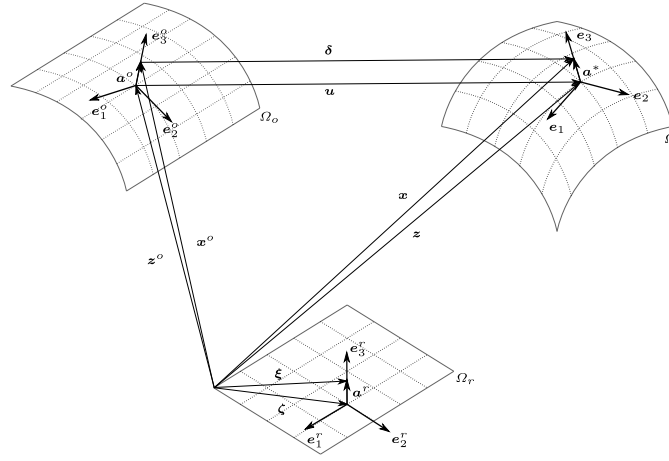


Figure 4: Shell configuration schematics.

basis, with e_α^r positioned tangent to the plane and e_3^r normal to it (if not stated otherwise, the usual index notation $\{i, j, k\} = [1, 2, 3]$ and $\{\alpha, \beta, \gamma\} = [1, 2]$ is adopted). In the reference plane, no curvatures are admitted. The position of any material point on the reference configuration can be obtained by

$$\boldsymbol{\xi} = \boldsymbol{\zeta} + \mathbf{a}^r, \quad (1)$$

where

$$\boldsymbol{\zeta} = \xi_\alpha e_\alpha^r, \quad (2)$$

is the mid-plane coordinate with $\xi_\alpha \in \Omega_r$ and

$$\mathbf{a}^r = \zeta e_3^r, \quad (3)$$

is the relative position along the thickness with $\zeta \in H^r = [-h/2, h/2]$.

The position of any material point along the initial configuration is given by

$$\mathbf{x}^o = \mathbf{z}^o + \mathbf{a}^o, \quad (4)$$

where, analogous to the reference configuration, \mathbf{z}^o defines the middle plane coordinate and

$$\mathbf{a}^o = \zeta e_3^o \quad (5)$$

its relative position along the thickness. The initial mapping is set to be of Kirchhoff–Love type, leading to

$$\mathbf{a}^o = \mathbf{Q}^o \mathbf{a}^r, \quad (6)$$

where \mathbf{Q}^o is the initial rotation tensor obtained by

$$\mathbf{Q}^o = e_i^o \otimes e_i^r. \quad (7)$$

The current configuration \mathbf{x} is described by

$$\mathbf{x} = \mathbf{z} + \mathbf{a}^*, \quad (8)$$

$$\mathbf{z} = \mathbf{z}^o + \mathbf{u}, \quad (9)$$

where \mathbf{z} is the mid-plane coordinate and \mathbf{u} the displacement vector. The mid-plane coordinate's relative position along the thickness is described by

$$\mathbf{a}^* = \left((1+p)\zeta + \frac{1}{2}q\zeta^2 \right) e_3, \quad (10)$$

where p and q are parameters introduced to govern the thickness variation on the current configuration.

The following equation can be used to relate the initial and reference configuration director

$$e_3 = Q^e e_3^o, \quad (11)$$

where Q^e is the effective rotation tensor. This tensor is analytically parametrized using the Euler–Rodrigues formula as

$$Q^e = I + h_1(\theta)\Theta + h_2(\theta)\Theta^2, \quad (12)$$

where I is the identity tensor, θ is the rotation vector, $h_1(\theta)$ and $h_2(\theta)$ are trigonometric functions, $\theta = \|\theta\|$ is the rotation angle and $\Theta = \text{skew}(\theta)$.

The previous kinematic assumption can now be introduced in the standard nonlinear continuum equations. The unknowns are the following functions parameterized along the reference configuration: the displacement vector, \mathbf{u} , the rotation vector, θ and the scalar parameters p and q . These eight unknown fields are discretized using the T6-3i finite element [5].

3.2 Thermo-visco-elasticity

For the beam material, we use a general thermo-visco-elasticity model, described by the rheological model illustrated in Figure 5, and written in the incremental variational framework described in [6].

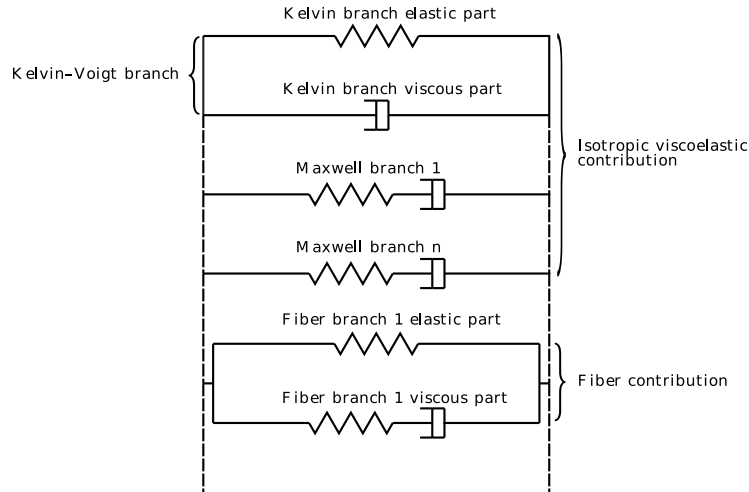


Figure 5: Rheological model.

Following the framework of Generalized Standard Materials, the model is described by a combination of a free energy potential $W(\mathbf{F}, \mathbf{Z}; T)$ and a dissipation pseudo-potential $\psi(\dot{\mathbf{F}}, \dot{\mathbf{Z}}; \mathbf{F}, \mathbf{Z}, T)$, where \mathbf{F} is the deformation gradient, $\mathbf{Z} = \{\mathbf{F}_1^v, \dots, \mathbf{F}_n^v, \mathbf{F}_f^v\}$ are the viscous deformation gradients corresponding to the n Maxwell branches, plus the fiber contribution, and T is the temperature (treated as an external parameter in this setting). The mechanical part of the model follows quite closely the structure proposed in [7], and is summarized below. The internal variable update over a time step $[t_n, t_{n+1}]$ is performed by minimizing an incremental potential

$$\mathbf{Z}_{n+1} = \arg \min_{\mathbf{Z}} [W(\mathbf{F}_{n+1}, \mathbf{Z}_{n+1}; T_{n+1}) - W(\mathbf{F}_n, \mathbf{Z}_n; T_n) + \Delta t \psi(\dot{\mathbf{F}}_{n,n+1}, \dot{\mathbf{Z}}_{n,n+1}; T_{n+\alpha})] \quad (13)$$

where $\dot{\mathbf{F}}_{n,n+1}$ and $\dot{\mathbf{Z}}_{n,n+1}$ are incremental approximations of the rates (not detailed here) and $\alpha \in [0, 1]$ is an algorithmic parameter. Both free energy and dissipation potentials are additively decomposed into an isotropic matrix contribution and a anisotropic fibre contribution. The free energy potential is given by

$$W(\mathbf{F}, \mathbf{Z}; T) = (1 - f) \left[\varphi(\hat{\mathbf{C}}; T) + U(J; T) + \sum_{i=1}^n \varphi_i^e(\hat{\mathbf{C}}_i^e; T) \right] + f \varphi_f^e(\mathbf{C}_f^e; T) \quad (14)$$

where $J = \det[\mathbf{F}]$, $\hat{\mathbf{F}} = J^{-\frac{1}{3}}\mathbf{F}$, $\hat{\mathbf{C}} = \hat{\mathbf{F}}^T \hat{\mathbf{F}}$, $\mathbf{F}_i^e = \mathbf{F}\mathbf{F}_i^v$, and f is the volume fraction of fibres. The potentials are of Hencky or Ogden type, following [6] and [7], with temperature-dependent elasticity moduli and thermo-elastic coupling. For the fibre contribution, we more specifically use a Hencky potential and the fibre stretch $\lambda_f^2 = \mathbf{C} : \mathbf{M}_f$, where $\mathbf{M}_f = \mathbf{n}_f \otimes \mathbf{n}_f$ is the material structural tensor. Similarly, the dissipation potential is written as

$$\psi(\dot{\mathbf{F}}, \dot{\mathbf{Z}}; \mathbf{F}, \mathbf{Z}, T) = (1 - f) \sum_{i=1}^n \psi_i(\mathbf{d}_i^v; T) + f \psi_f(d_f^v; T) \quad (15)$$

where $\mathbf{d}_i^v = \dot{\mathbf{F}}_i^v \mathbf{F}_i^{v-1}$ and $d_f^v = \dot{\lambda}_f / \lambda_f$ are the viscous strain rates. The model was implemented in MATLAB [4].

4 Numerical examples

In this section we present a test case application of the full thermo-mechanical model described above. The model is applied to the GFRP tubular component named Ultra Duty PlanckTM, commercialized by Fiberline Building Profiles (a more detailed geometrical description of the component can be found at the company's website [8]). Unfortunately, the available material data for this component is significantly scarce, specially under elevated temperatures. Nonetheless, we can still obtain representative results by roughly estimating these properties.

The 2D thermal Finite Element mesh used in the simulations was generated using Gmsh [9] and is illustrated in Figure 6. The local refinement near the cavity walls is applied so that the fluid boundary layer is accurately captured. Also using Gmsh, the 3D mechanical mesh was generated by extracting and extruding the mid-surface of the profile's section walls.

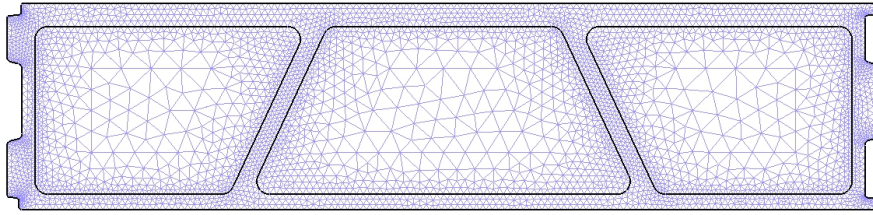


Figure 6: Thermal model test case mesh.

The thermal part boundary conditions follow the schematic representation shown in Figure 3. For the mechanical problem, the tubular component is set to be simply supported with two loads applied to its top surface.

Sample results for the thermal part of the problem can be seen in Figures 7 and 8. As the fire temperature increases, heat enters the profile (by convection and radiation) and spreads into the material through conduction. As it reaches the inner cavities, it gets transferred to the air, causing a temperature gradient and generating a natural convection phenomenon. Whenever the internal walls temperature gets high enough, internal radiation also becomes non-negligible, contributing to the overall heating of the material's top flange. In its solid part, the high temperatures cause the material to decompose. At the final stages of the simulation, the material reaches a quasi steady state condition, with the temperature well spread throughout the profile and its walls almost fully decomposed.

Sample results for the mechanical part of the problem are shown in Figure 9. The deformed components are presented at 3 different time instants with their corresponding profile temperatures on the top. As the temperature increases at the bottom flange, the material's mechanical properties start to degrade and the overall displacement increases. Thermal dilation and viscous (creep) effects also play important roles on the overall displacement increase. Notice that all these phenomena occur at a constant mechanical load, applied in the first time increment.

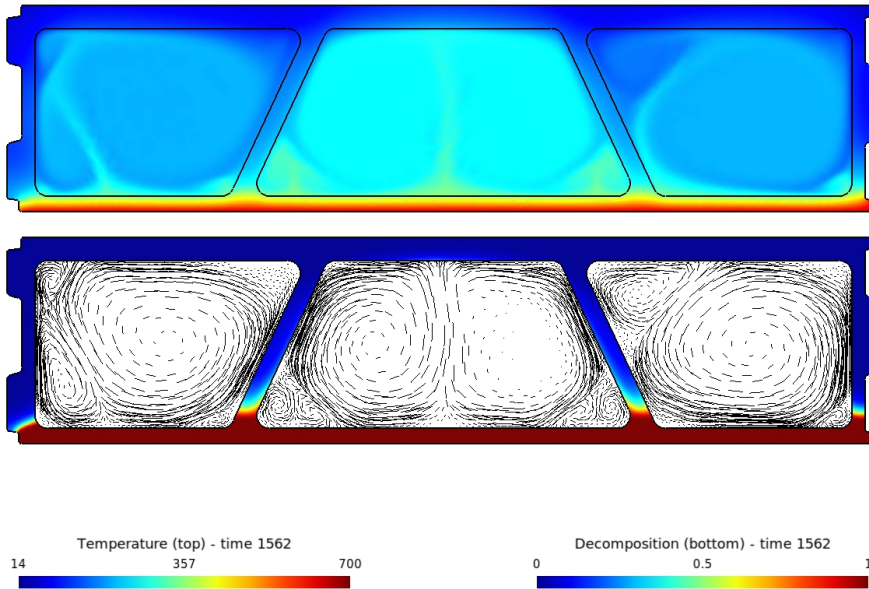


Figure 7: Thermal model test case results at intermediate time.

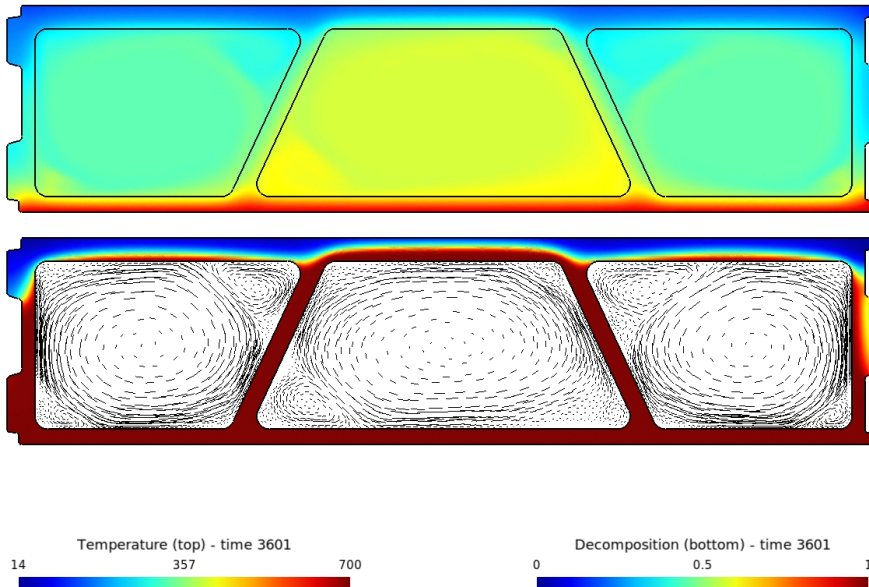


Figure 8: Thermal model test case results at final time.

5 Conclusion

In this work we presented a thermo-mechanical model developed for the simulation of pultruded GFRP profiles under the influence of a standard fire curve. As mentioned, the problem is separated into two main parts:

- (i) The thermal problem is solved for a representative 2D profile section including conduction, internal convection and internal radiation.
- (ii) Using the temperature results provided by the thermal problem, the mechanical problem is solved using a geometrically exact thick shell theory in conjunction with a thermo-visco-elastic 3D constitutive model.

A test case application considering a commercial GFRP profile under a fire curve was presented along with its corresponding thermal and mechanical results. Considering the lack of material data,

the model is already showing very promising results, which should be further improved as more data becomes available.

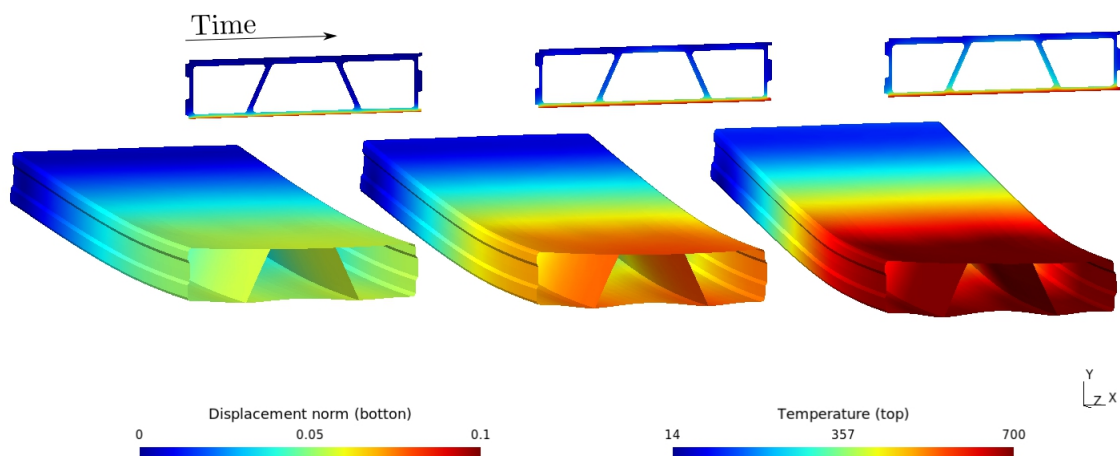


Figure 9: Mechanical model results for three distinct time instants.

References

- [1] C. Lopez *Numerical modelling of the thermomechanical behaviour of GFRP pultruded profiles subjected to fire*, Ph.D. thesis, Instituto Superior Técnico, University of Lisbon, Lisbon, Portugal, 2017.
- [2] T. Morgado, N. Silvestre, J. R. Correia, F. A. Branco, T. Keller *Numerical modelling of the thermal response of pultruded GFRP tubular profiles subjected to fire*, *Composites Part B: Engineering*, 137, 202-216, 2018.
- [3] T. Morgado, J. R. Correia, N. Silvestre, F. A. Branco *Experimental study on the fire resistance of GFRP pultruded tubular beams*, *Composites Part B: Engineering*, 139, 106-116, 2018.
- [4] L. Stainier, F. Dubois, R. Peyroux *MatLib, une bibliothèque portable de modèles constitutifs pour la mécanique non-linéaire des solides: concepts et implémentation*, 6ème Colloque National en Calcul des Structures, 3, 25–32, 2003.
- [5] P. M. Pimenta, E. M. B. Campello, P. Wriggers *A fully nonlinear multi-parameter shell model with thickness variation and a triangular shell finite element*, *Computational Mechanics*, 34(3), 181–193, 2004.
- [6] L. Stainier *A Variational Approach to Modeling Coupled Thermo-Mechanical Nonlinear Dissipative Behaviors*, *Advances in Applied Mechanics*, 46, 69–126, 2013.
- [7] J. M. Vassoler, L. Stainier, E. A. Fancello *A variational framework for fiber-reinforced viscoelastic soft tissues including damage*, *International Journal for Numerical Methods in Engineering*, 108(8), 865–884, 2016.
- [8] Fiberline Building Profiles, website: www.fiberline.com, visited on 11-12-2021.
- [9] C. Geuzaine, J.-F. Remacle *Gmsh: a three-dimensional finite element mesh generator with built-in pre- and post-processing facilities*, *International Journal for Numerical Methods in Engineering* 79(11), 1309-1331, 2009.